

3D Radiation Detectors: Charge Collection Characterisation and Applicability of Technology for Microdosimetry.

Linh T. Tran, *Student Member, IEEE*, Dale A. Prokopovich, Marco Petasecca, *Member, IEEE*, Michael L. F. Lerch, *Member, IEEE*, Angela Kok, Anand Summanwar, Thor-Erik Hansen, Cinzia Da Via, Mark I. Reinhard, *Member, IEEE* and Anatoly B. Rosenfeld, *SeniorMember, IEEE*

Abstract— A study of charge collection in SINTEF 3D active edge silicon detectors was carried out at ANSTO using Ion Beam Induced Charge (IBIC) technique. An IBIC study has shown that several different geometries of 3D detectors have full depletion under low applied bias. The effect of fast neutron and gamma radiation on their charge collection efficiency was also investigated. A 3D active edge silicon detector technology has demonstrated extremely promising performance for application of the 3D Sensitive Volumes (SVs) fabrication methods to SOI microdosimetry.

Index Terms—Microdosimetry, 3D detector, radiation damage, charge collection, IBIC.

I. INTRODUCTION

THE microdosimetric approach involves measuring the stochastic lineal energy deposition, on an event-by-event basis. The energy depositions are, on a micron scale sensitive target volume (SV), comparable to human cell dimensions. These events arise from charged particles traversing the SV from either the primary radiation field or from secondary particles originating via nuclear interactions within the surrounding material. Using microdosimetry it is possible to be able to deduce the dose equivalent in any arbitrary mixed radiation field [1]. This is a major advantage over the other dosimetry methods that can only measure the absorbed dose or require prior knowledge of the field composition.

Conventional microdosimeter uses a tissue equivalent proportional counter (TEPC) that incorporates a spherical SV filled with tissue equivalent gas and is able to model a micron sized biological cell by using low pressures. The TEPC has several limitations including high voltage operation, large size (i.e. poor spatial resolution), and is only able to mimic a single, isolated cell [2]. The solid state microdosimeter was

proposed as a new method of measuring the energy deposition in an array of micron sized SVs [2, 3].

The Centre for Medical Radiation Physics (CMRP) has developed three generations of microdosimeters based on silicon-on-insulator (SOI) substrates [4-8]. These SOI microdosimeters were based on planar and pseudo 3D mesa rectangular parallelepiped (RPP) and cylindrical SVs produced on p-SOI and n-SOI using diffusion or implantation techniques for forming laterally depleted p-i-n diodes. However, the previous generations have had lateral charge diffusion from outside the SVs in the device. The diffusion charge collection compromises the definition of the SV increasing the uncertainty in the microdosimetric parameters, such as an average chord and chords variance.

In order to address these challenges, CMRP has proposed design of optimal SOI microdosimeter with free standing true 3D “mushroom” SVs. Three dimensional (3D) SVs embedded in polymethyl methacrylate (PMMA) can be fabricated using 3D detector technology via state-of-the-art silicon processing facilities which are well established at SINTEF MiNaLab, Oslo, Norway. Fabrication of new SOI microdosimeters is a significant step forward in radiation dosimetry for radiation protection in space, avionics, and radiation therapy applications.

The 3D detector concept was first proposed by S. Parker in 1995 and the active edge detector technology was proposed by C. Kenney in 1997. The developments of micro-machining and standard VLSI (Very Large Scale Integration) technologies, together with advanced technology - Deep Reactive Ion Etching (DRIE) make 3D detector fabrication possible [9]. 3D electrodes are achieved by precisely drilling cylindrical micro-holes in a silicon wafer using DRIE technology, which includes an inductively-coupled plasma etching and a sidewall passivation [10]. These holes are then filled with conductive boron or phosphorus doped polycrystalline silicon.

Another important feature of the 3D detector is an active edge technology, which can be used in fabrication of the 3D SV for microdosimeters [11]. A principle of etching 3D technology is shown in Fig.1.

In 2008 SINTEF MiNaLab was the second laboratory in the world that has successfully explored and fabricated the 3D detectors with the active edges on a small production scale [12, 14].

L. T. Tran, M. Petasecca, M. L. F. Lerch and A. B. Rosenfeld are with the Centre for Medical Radiation Physics, University of Wollongong, NSW 2522, Australia (e-mail: lt822@uowmail.edu.au; marcop@uow.edu.au, m1erch@uow.edu.au; anatoly@uow.edu.au).

D. A. Prokopovich and M. I. Reinhard are with the Institute of Materials Engineering, Australian Nuclear Science and Technology Organisation, Lucas Heights, NSW2234, Australia (e-mail: dpr@ansto.gov.au; mrz@ansto.gov.au).

A.Kok and A.Summanwar are with the SINTEF MiNaLab, SINTEF, Oslo, Norway (email: angela.kok@sintef.no; Anand.Summanwar@sintef.no).

C. Da Via is with the University of Manchester, UK (email: Cinzia.Da.Via@cern.ch).

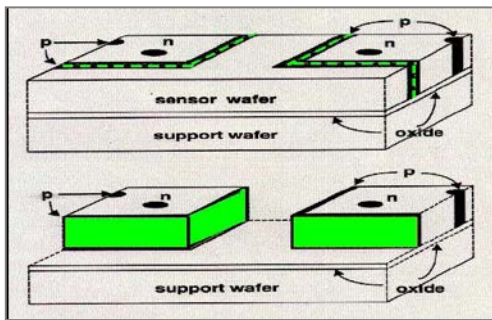


Fig. 1. Processing of 3D active edge detector (image was adapted from [12])

Based on advanced technologies available in fabrication 3D detectors with the active edge, we have embarked on a research project on fabrication of the 3D silicon-based Mushroom microdosimeter for radiation therapy and radiation protection applications in space, avionics, and terrestrial applications. The mushroom silicon microdosimeter will be exposed to a harsh mixed radiation environment that can affect the charge collection efficiency in the 3D SVs and result in an error in measured dose equivalent. Current research is focused on the study of charge collection in the 3D Si detectors, which currently utilize the technology aimed for the mushroom SVs fabrication. The effect of fast neutron and gamma radiation on the 3D detector charge collection efficiency is used to quantify the radiation sensitivity of this design. Previous study on the radiation hardness of similar 3D detectors produced at the Stanford Nanofabrication Facility was performed using an infrared (IR) laser to inject the equivalent of approximately 2 minimum ionizing particles. These experiments demonstrated charge collection efficiencies as high as 66% after irradiation of detectors with neutrons up to a fluence $8.8 \times 10^{15} \text{ n}_{\text{eq}}/\text{cm}^2$, for a $56 \mu\text{m}$ inter-electrode [15]. The proposed IBIC technique has much higher spatial resolution than the IR laser technique and will provide an accurate and fast 2D charge collection efficiency map in the 3D SINTEF detectors with spatial resolution approximately $1 \mu\text{m}$. IBIC gives the advantage of being able to observe details associated with radiation damage which were not earlier observed with IR laser as well as being able to tailor the depth and energy of the deposition event.

II. MATERIAL AND METHOD

A. Test structure of SINTEF 3D detectors

The SINTEF 3D detectors were fabricated on $10 \text{ k}\Omega\cdot\text{cm}$ p-Si wafer with $1 \text{ mm} \times 1 \text{ mm}$ dimensions and a thickness of $285 \mu\text{m}$ as a part of the ATLAS collaboration. Fig. 2 shows the layout of the metal contacts and passivation openings on the test 3D detector. Five detectors with different inter-electrode distances between the centers of n^+ and neighboring p^+ electrodes of 3D detectors were investigated. Each pixel consists of one 3D n^+ -type electrode (1E configuration), two n^+ -type electrodes (2E configuration), three n^+ -type electrodes (3E), four n^+ -type electrodes (4E) and five n^+ -type electrodes (5E). The inter-electrode distances corresponding to each type of detectors 1E, 2E, 3E, 4E and 5E are $200 \mu\text{m}$, $104 \mu\text{m}$, $70 \mu\text{m}$, $56 \mu\text{m}$ and $46 \mu\text{m}$, respectively. Each group of n^+ electrodes has its own bond pad, while p^+ electrodes and an active p^+ edge are connected in parallel.

B. Electrical Characterisation

The electrical properties of each detector was determined using current-voltage (I-V) and capacitance-voltage (C-V) measurements with a Keithley 237 high voltage source measure unit and Botoon 7200 capacitance bridge. All measurements were carried out under controlled ambient room temperature of 20°C .

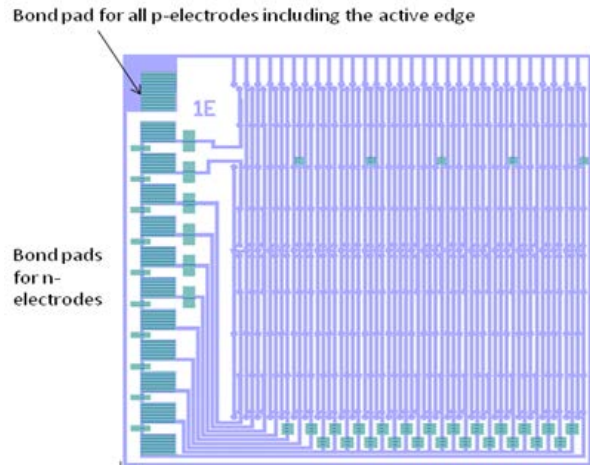


Fig. 2 Layout of the of the test diode

C. Charge Collection Study

The charge collection efficiency for the different types of the 3D detectors was investigated using the IBIC technique on the Heavy Ion Microprobe at ANSTO [13]. The IBIC measurements utilized a microbeam of 5.5 MeV He^{2+} ions focused to a diameter of approximately $1 \mu\text{m}$ which was raster scanned over the surface of the sample. The amount of energy deposited in the 3D detectors was measured using an AMPTEK A250 charge sensitive preamplifier and Canberra 2025 Shaping Amplifier with $1 \mu\text{s}$ shaping time. The signal was fed directly to a Canberra 8701 analog to digital converter (ADC) of the data acquisition system. The IBIC signal corresponding to the beam position “x” and “y” as well as the charge collection “E” for each event was processed into an event-by-event list mode file. The data was processed into IBIC median charge collection image maps for spatial correlation of the energy deposition of the scanned area. The energy calibration was performed using a calibrated pulse generator which was calibrated to a $300 \mu\text{m}$ thick planar silicon PIN diode with 100% Charge Collection Efficiency (CCE) in response to an ^{241}Am source.

D. Radiation Damage Study

Effect of 10 MRad gamma radiation and $6.2 \times 10^{10} \text{ n}_{\text{eq}}/\text{cm}^2$ fast neutrons on the charge collection efficiency of 3D detectors was investigated using the Gamma Technology Research Irradiator (GATRI) at ANSTO and 10 Ci Am-Be source at Commonwealth Scientific and Industrial Research Organisation (CSIRO) research facilities.

III. RESULTS AND DISCUSSIONS

A. Electrical Characterisation

The 3D detectors with longer inter-electrode distance (1E, 2E and 3E type) have reverse current less than 80 nA at 100 V

while the detectors with shorter inter-electrode distance (4E and 5E) have higher reverse current (about 300 nA at 80 V). The graph of capacitance at 60 V bias versus inter-electrode distance (Fig. 3) shows that for shorter inter-electrode distance for the same size of the test diode significantly raises the capacitance.

B. Charge Collection Study

The 3D detector was scanned with 5.5 MeV He^{2+} ions microbeam at different locations. Fig. 4a, b show scanned area and Multichannel Analyzer (MCA) spectra in 3D detector type 1E with 200 μm inter electrode distance for 0 V and 100 V bias, respectively. All n^+ electrodes were connected in parallel.

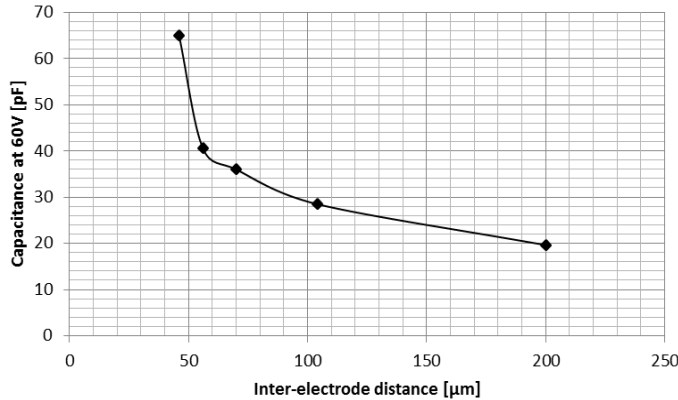


Fig. 3 Capacitance of different types of 3D detectors at 60V.

Fig 4c, d show the median energy maps of collected charge for this scanned area under the same conditions. Even under 0 V bias, the 3D detector with the largest inter-electrode distance has reasonable diffused charge collection with almost 100% near n^+ electrodes. For 100 V bias, full charge collection has been observed through all scanned area limited by active p^+ edge of the 3D detector.

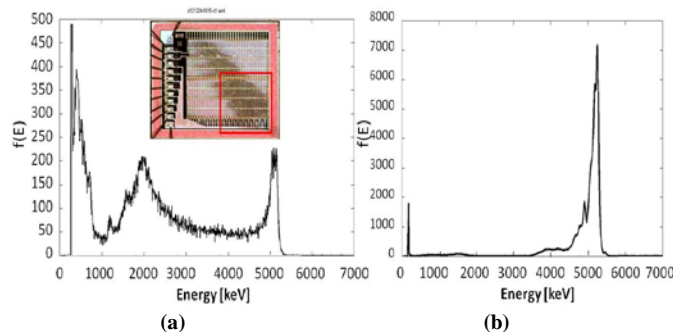


Fig. 4 Scanned area of 1E 3D detector and MCA spectra at (a) 0 V bias and (b) 100 V bias.

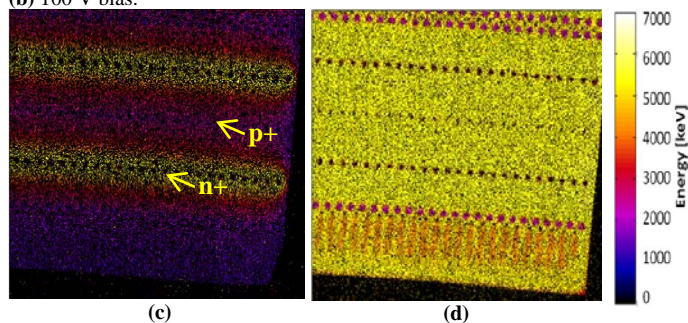


Fig.4. An IBIC median energy map of the response of 3D detector (1E type) to the microbeam of 5.5 MeV He^{2+} (c) at 0 V and (d) at 100 V.

This is also reflected in the MCA spectra in Fig 4b. A small low energy satellite peak is due to the losses of energy by He^{2+} ions traveling through Al tracks connecting n^+ and p^+ electrodes and above p^+ active edge on the periphery of the 3D detector.

At 100 V bias, the 3D detector has much better energy resolution than for 0 V bias and it can be seen fine structure of two small peaks appeared on the left side of the main peak. It is due to two different thicknesses of overlayers including metallization and oxide on p^+ columns at the bottom of the chip and outside of p^+ columns (Fig. 5b, c). Fig. 5b shows nearly full depleted region on the edge of the detector and demonstrates edgeless detector performance. Uniform full charge collection between n^+ and p^+ electrodes was observed at 100 V as presented in a Fig 5d. Figures 5a-d were obtained using the energy windows corresponding to the features on a MCA spectrum.

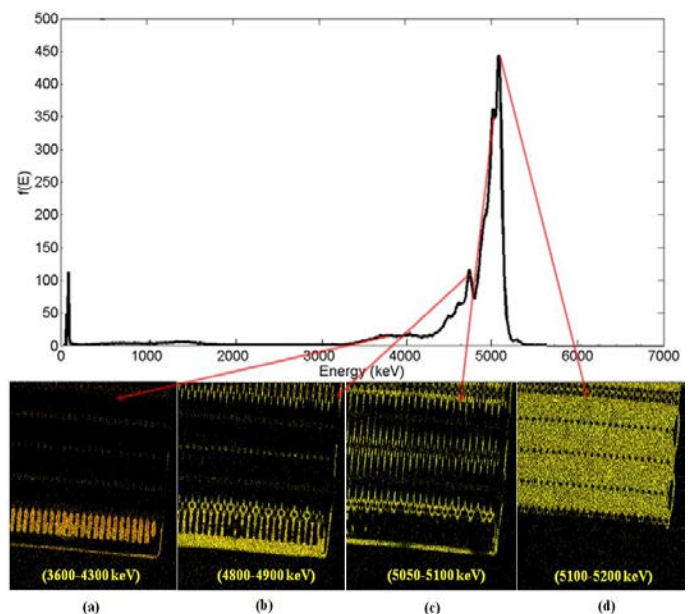


Fig. 5. Median energy maps in different energy ranges of charge collection of 1E detector at bias 100 V.

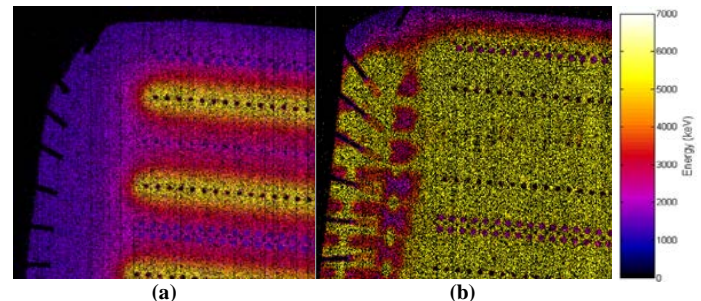


Fig.6. An IBIC median energy map of the response of the 3D detector 1E at the top left corner to the microbeam of 5.5 MeV He^{2+} (a) at 0 V and (b) at 100 V.

Fig. 6 illustrates the charge collection for the same scan size in the upper left corner of the 1E 3D detector under the same bias conditions. Bonding wires are clearly observed on both charge collection images. A magnified view of the median energy map allows one to confirm the full depletion through the 3D detector volume and the excellent performance of the active edge. The regions with deficit of the deposited energy from He^{2+} ions are observed under the Al contact pads

and Al deposited above an active p^+ edge due to energy loss in Al contacts (Fig. 6b).

Fig. 7 shows an enlarge median energy map of n^+ and p^+ electrodes in the middle of the chip for type 2E with 104 μm inter-electrode distance. While both p^+ and n^+ 3D electrodes were produced of the same diameter, their effective diameters in terms of charge collection are different, which have been also observed in 1E detector. The effective diameter of n^+ column with zero charge collection (black color, Fig 7) is about 22 μm , while p^+ column has an effective diameter of 13 μm under zero bias. Similarly as for the 3D detector type 1E, an excellent charge collection has been demonstrated for the detector type 2E under 100 V bias (Fig. 8b). In Fig. 8 b, details of a wire compression during the wire bonding were also observed. Part of the bonding wires becomes thinner due to compression so that alpha particle has lost less energy in these regions. Full depletion between wire contacts compression regions can be seen. Under full depletion at 100 V, the bottom edge was fully depleted.

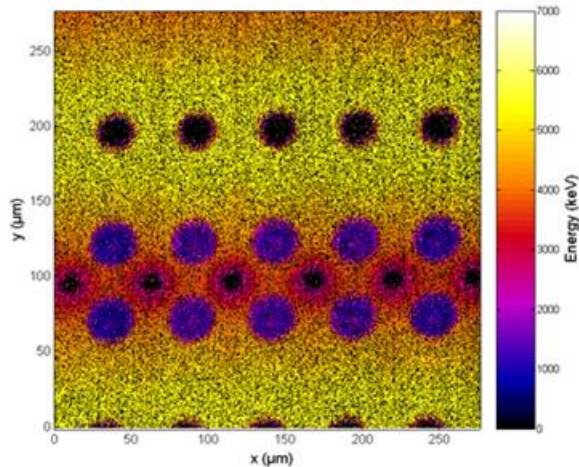


Fig.7. An IBIC enlarge median energy map of 2E detector in response to 5.5 MeV He^{2+} at 0 V.

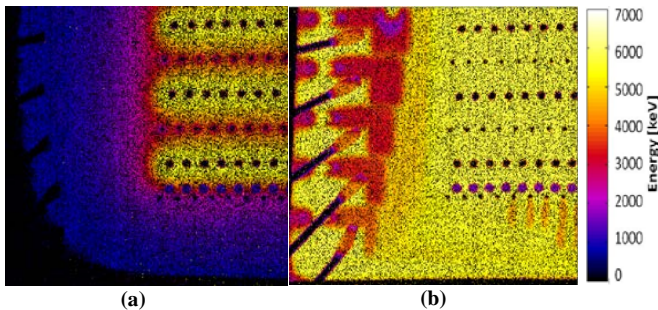


Fig.8. An IBIC median energy map of the response of detector 2E at the bottom left side to the microbeam of 5.5MeV He^{2+} (a) at 0 V and (b) at 100 V.

Fig. 9 shows the charge collection in one part of the 3D detector type 3E in response to 5.5 MeV He^{2+} ions. It is observed that the charge collection is changing with bias. It can be seen that at 0 V, detector type 3E with an inter-electrode distance 70 μm has lower energy events near the bottom edge of the chip (Fig. 9a). With increasing bias applied to the detector, the Al contacts which connecting n^+ columns to the bonding pads became visible with lower charge collection (red region at the edge of the chip, Fig. 9b, c). At 90 V, the detector was fully depleted near the edge and it can be seen that slightly lower charge collection along Al leads near

the edge is due to energy loss by alpha particles in Al metallization (Fig. 9f). IBIC images are demonstrating degraded charge collection on a border of p^+ .

Fig. 10 shows a median energy charge collection image for the 3D detector type 5E which has shortest inter-electrode distance of 46 μm . Full charge collection through the 3D detector volume was observed at a bias as low as 5 V. The effective diameters of n^+ and p^+ columns (black region) are approximately 22 μm and 13 μm , respectively with a clear observation of diffusion charge collection from inwards of the p^+ 3D electrodes (Fig. 10a) as in other 3D diodes. The difference in the effective diameters of p^+ and n^+ electrodes observed in all 3D diodes from this batch is possibly caused by the difference in the radial distribution of resistivity of the filled polysilicon doped with phosphorous and boron, the physical size of the electrodes due to the variations in the fabrication process.

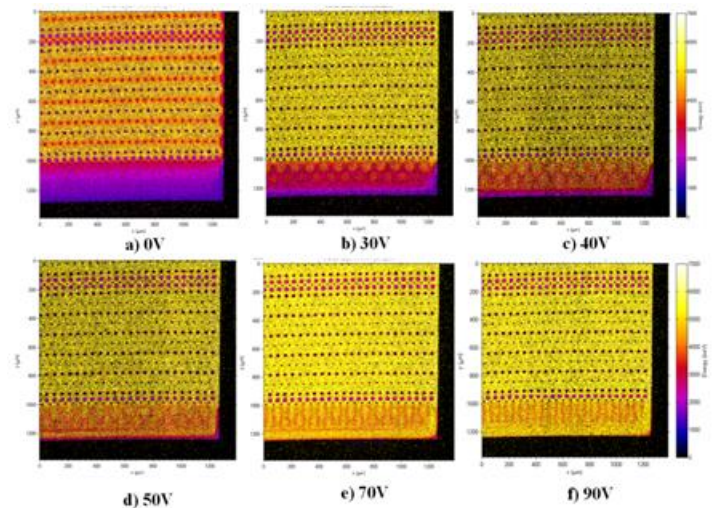


Fig. 9. An IBIC median energy map comparison of 3D detector type 3E in response to 5.5 MeV He^{2+} at different biases a) 0 V, b) 30 V, c) 40 V, d) 50 V, e) 70 V and f) 90 V.

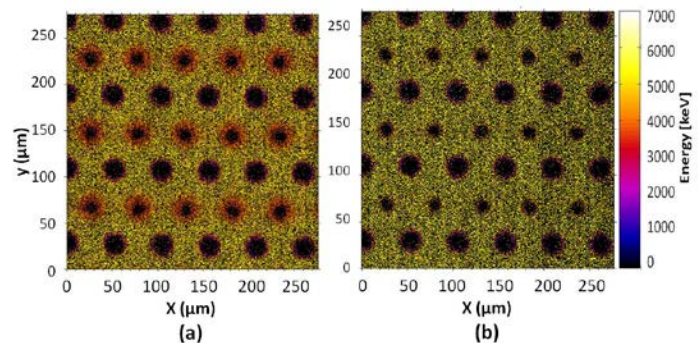


Fig.10. An IBIC enlarge median energy map of 5E detector in response to 5.5 MeV He^{2+} at a) 0 V and b) 5 V.

Fig. 11 shows a MCA spectrum and a median energy map for the energy window corresponding to the major peak 5100-5300 keV and representing 100% of the charge collection. It was clear demonstrating the same diameter of n^+ and p^+ electrodes and supporting explanation of diffused charge collection from inside of p^+ electrode. Based on obtained results, it is suggested that the resistivity of p^+ columns must be not as low as n^+ columns.

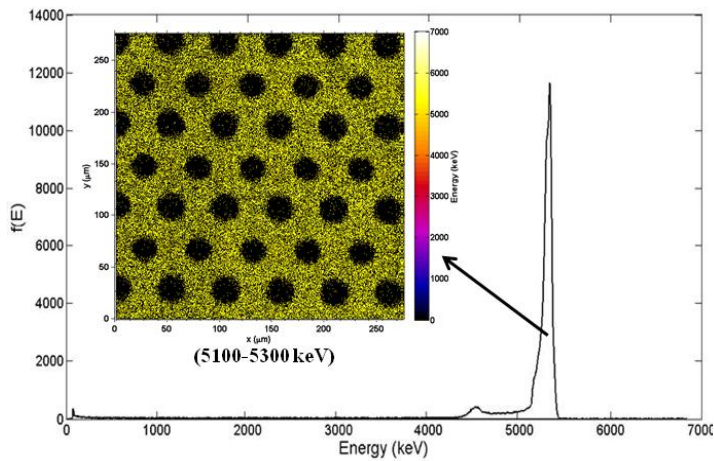


Fig. 11. An IBIC MCA spectrum and median energy map of the charge collection of 5E type detector at bias 5 V for energy window (5100-5300 keV)

C. Radiation Damage Study

An I-V characterisation for the 3D detectors before and after irradiation was carried out. Fig. 11 shows the leakage current in the 3D detectors type 1E, 3E, 5E before and after gamma irradiation. The leakage current of the detector type 1E has increased from 20 nA to approximately 180 nA at 80 V.

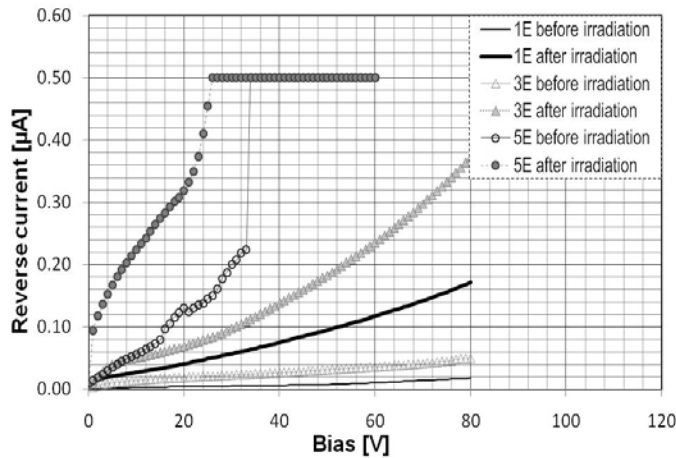


Fig. 12. An I-V characteristic comparison for 3D detectors type 1E, 3E, 5E before and after 10 MRad gamma ^{60}Co irradiation.

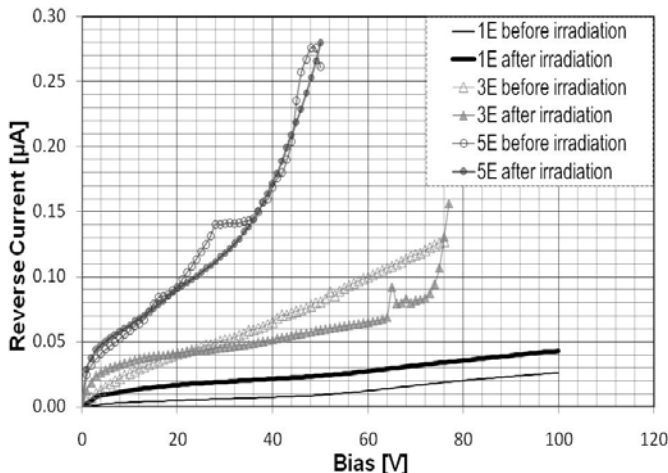


Fig. 13. An I-V characteristic comparison for 3D detectors type 1E, 3E, 5E before and after neutron irradiation with fluence of $6.2 \times 10^{10} \text{ n}_{\text{eq}}/\text{cm}^2$.

Slightly change of the leakage current has been observed for the neutron irradiated samples that is in agreement with low neutron fluence. The previous study of the charge collection efficiency of the 3D detectors has been shown that the longer inter-electrode distances samples were less radiation hard than the shorter inter-electrode ones [15]. The IBIC results provide detailed effects of the charge collection after a small fluence of $6.2 \times 10^{10} \text{ n}_{\text{eq}}/\text{cm}^2$ of fast neutrons and 10 MRad ^{60}Co gamma irradiation. Two gamma irradiated (3E, 5E) and three neutron irradiated (1E, 3E and 5E) 3D detectors have been chosen for investigation by the IBIC technique.

Fig. 14 shows a comparison of the MCA spectra and the median energy maps with 1 x scan size for the 3D detectors type 3E at bias 60 V before and after gamma irradiation. It can be seen that slightly lower energy charge were collected between and along p^+ columns. It is due to an accumulation of positive charges in the SiO_2 layer, which is changing electrical field distribution near the surface of the P-type silicon- SiO_2 and effected the charge collection produced by short range He^{2+} ions. This build up charge is also leading to essential increasing of reverse current in this diode as observed in a Fig. 12.

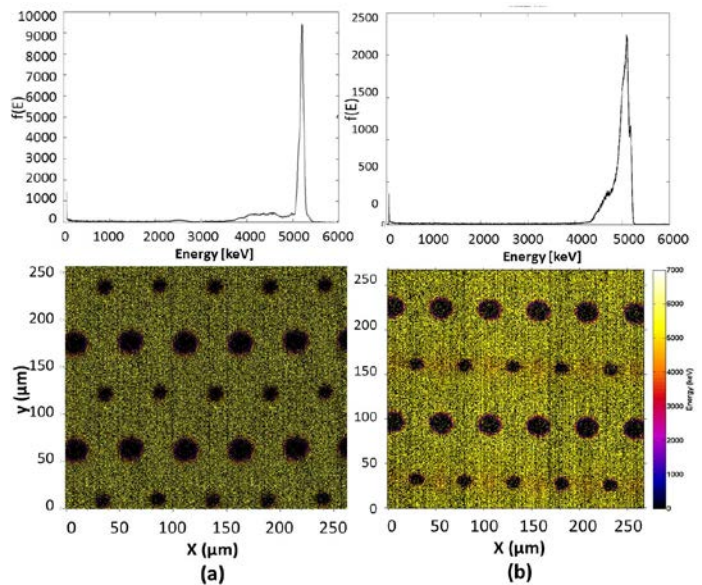


Fig.14. IBIC MCA spectra and median energy maps for gamma irradiated sample (3E type) at bias 60V a) before irradiation b) after gamma irradiation

Fig. 15 shows a comparison of the MCA spectra and the median energy maps with 5 x scan size for 3D detectors type 1E at 100 V before and after neutron irradiation. In Fig. 15b, the lower charge collection regions were observed near the p^+ electrodes (red region) in comparison with region around n^+ electrodes (yellow region). Statistics of these events are comparable with the statistics of higher energy events near n^+ columns (2 peaks with almost the same amplitude can be seen in the MCA spectrum). The regions near p^+ electrodes were not fully depleted even at 100 V. Deficit in charge collection associated with a lower energy peak is explained by bulk neutron radiation damage and larger charge recombination due to induced radiation defects and related to them recombination centers. This is agreement with [15] as 1E diode has largest inter-electrode distance. The effect of build up charge in the oxide in this case is minimal due to much lower gamma dose

during neutron irradiation in comparison with irradiation on a ^{60}Co source. A more detailed IBIC investigation is required with protons penetrating through 285 μm thickness of the detector. This will ensure that the energy deposition is only due to transient radiation that is not stopped within the sensitive volume.

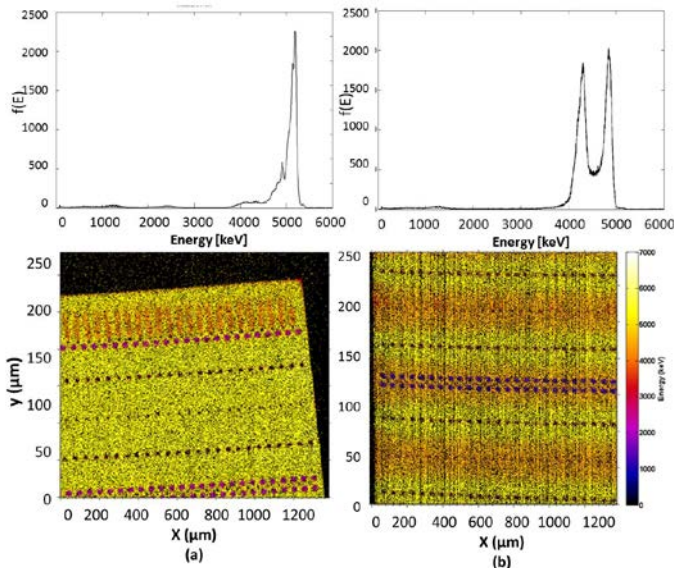


Fig.15. IBIC MCA spectra and median energy maps for neutron irradiated sample (1E type) at bias 100 V; a) before irradiation b) after neutron irradiation

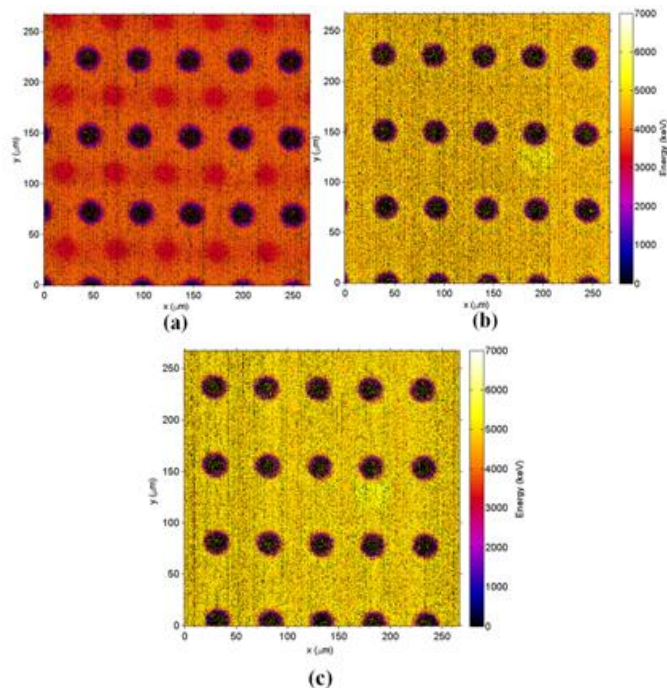


Fig.16. IBIC median energy maps at 1x scan size for gamma irradiated sample (5E) at biases a) 0 V, b) 10 V and c) 30 V.

Abnormal effect of the buildup positive charge has been observed on 5E 3D detectors with shortest 46 μm inter-electrode distance irradiated with 10 MRad ^{60}Co gamma. Fig 16a, b, and c show the median energy map for this detector for biases 0 V, 10 V, and 30 V. While full depletion was achieved under 10 V bias, no p^+ electrodes has been observed. It is supporting hypothesis of negative inverse layers on the surface

of the detector responsible for charge collection close to the surface. This inverse layer is not effected absence of charge collection in n^+ electrodes presented as black holes on images on Fig 16. There are no remarkable changes in bulk charge collection efficiency in 3E and 5E devices after irradiation at these dose levels. It makes us comfortable that for small 3D SVs of SOI mushroom microdosimeter we are not going to observe effect of radiation damage for higher doses of gamma and neutron irradiation.

IV. CONCLUSIONS

Charge collection in the SINTEF 3D detectors was investigated. An IBIC study has shown that different types of 3D detectors have full depletion under low applied bias. 3D silicon detector technologies and active edge detector have demonstrated extremely promising performance for applying for mushroom microdosimeter fabrication.

The IBIC technology is extremely sensitive to alternations in charge collection and has high spatial resolution of about 2 μm . The radiation damage study of irradiated 3D detectors has demonstrated that 3D detectors have no significant damage in terms of charge collection after 10 MRad gamma irradiation. Detector with longest inter-electrode distance has been shown with slightly lower charge collections at low fluence of neutrons. Build up positive charge is effecting on distribution of potential close to the detector surface between p^+ and n^+ electrodes that is effecting lateral charge collection for short range particles.

3D technology has been demonstrated extremely promising in application in microdosimetry and it will be a step forward in development of SOI microdosimeters applied in radiation protection and heavy ion therapy.

ACKNOWLEDGMENT

The authors would like to acknowledge the support of the Accelerator Operation Team, Institute of Environmental Research, Australian Nuclear Science and Technology Organization (ANSTO) for IBIC experiments and 3D MiMiC collaboration.

REFERENCES

- [1] ICRU, (1986). "The Quality Factor in Radiation Protection", *ICRU Report 40*.
- [2] A. B. Rosenfeld, P. D. Bradley, I. Cornelius, B. J. Allen, M. Zaider, R. L. Maughan, J. C. Yanch, J. Coderre, J. B. Flanz, and T. Kobayashi, "Solid state microdosimetry in hadron therapy," *Radiat. Protect. Dosim.* vol. 101, pp. 431–434, 2002.
- [3] P. Bradley, "The development of a novel silicon microdosimeter for High LET radiation therapy," *Ph.D. Thesis*, University of Wollongong, Wollongong, Australia, 2000.
- [4] P. D. Bradley, A. Rosenfeld, B. Allen, J. Coderre, and J. Capala, "Performance of silicon microdosimetry detectors in boron neutron capture therapy," *Radiat. Res.*, vol. 151, pp. 235–243, 1999.
- [5] I. Cornelius and A. Rosenfeld, "Verification of Monte Carlo calculations in fast neutron therapy using silicon microdosimetry," *IEEE Trans. Nucl. Sci.*, vol. 51, no. 3, pp. 873–877, Jun. 2004.
- [6] I. M. Cornelius, A. B. Rosenfeld, R. Seigele, and D. Cohen, "LET dependence of the charge collection efficiency of silicon microdosimeters," *IEEE Trans. Nucl. Sci.*, vol. 50, no. 6, pp. 2373–2379, Dec. 2003.
- [7] W.H. Lim, A. L. Ziebell, M. I. Reinhard, I. Cornelius, D. A. Prokopovich, A. S. Dzuras, and A. B. Rosenfeld, "Cylindrical Silicon-on-Insulator Microdosimeter: Design, Fabrication and TCAD modelling", *IEEE Trans. Nucl. Sci.*, NS-56,424-428, 2009.

- [8] Livingstone, D. A. Prokopovich, M. L. F. Lerch, M. Petasecca, M. I. Reinhard, H. Yasuda, M. Zaider, J. Ziegler, V. L. Pisacane, J. Dicello, V. Perevetaylo and A. B. Rosenfeld, "Large Area Silicon Microdosimeter for Dosimetry in High LET Space Radiation Fields: Charge Collection Study", *IEEE Trans. Nucl. Sci.*, 59, 3126-3132, 2012.
- [9] I. Parker, C. J. Kenney, and J. Segal, "3D- A proposed new architecture for solid-state radiation detectors," *Nucl. Instrum. Meth. Phys. Res. A*, vol. A395, pp. 328–343, 1997.
- [10] T. E. Hansen, A. Kok, T. A. Hansen, N. Lietaer, M. Mielnik, P. Storas, C. DaVia, J. Hasi, C. Kenney, and S. Parker, "First fabrication of full 3D- detectors at SINTEF," *J. Inst.*, vol. 4, p. P03010, 2009.
- [11] C. J. Kenney, J. D. Segal, E. West Brook, S. Parker, J. Hasi, C. Da Via, S. Watts, and J. Morse, "Active-edge planar radiation sensors," *Nucl. Instrum. Meth. Phys. Res. A*, vol. A565, no. 1, pp. 272–277, 2006.
- [12] A. Kok, G. Anelli, C. Da Via, J. Hasi, P. Jarron, C. Kenny, J. Morse, S. Parker, J. Segal, S. Watts, and E. Westbrook, "3D detectors—State of the art," *Nucl. Instrum. Meth. Phys. Res. A*, vol. A560, no. 1, pp. 127–130, 2006.
- [13] R. Siegele, D. Cohem, and N. Dytlewski, "The ANSTO high energy heavy ion microprobe," *Nucl. Instrum. Meth. Phys. Res. B*, vol. 158, pp. 31–38, 1999.
- [14] Cinzia Da Via, Maurizio Boscardin, Gian-Franco DallaBetta, Giovanni Darbo, Celeste Fleta, Claudia Gemme, Philippe Grenier, Sebastian Grinstein, Thor-Erik Hansen, Jasmine Hasi, Chris Kenney, Angela Kok, Sherwood Parker, GiulioPellegrini, Elisa Vianello, Nicola Zorzi."3D silicon sensors: Design, large area production and quality assurance for the ATLAS IBL pixel detector upgrade". *Nucl. Instrum. Meth. Phys. Res. A*, vol 694, pp. 321–330, 2012.
- [15] C. Da Via, E. Bolle, K. Einsweiler, M. Garcia-Sciveres, J. Hasi, C. Kenney, V. Linhart, Sherwood Parker, S. Pospisil, O. Rohne, T. Slavicek, S. Watts, N. Wermes, "3D active edge silicon sensors with different electrode configurations: Radiation hardness and noise performance" , *Nucl. Instrum. Meth. Phys. Res. A*, vol 604, pp. 505–511, 2009.